Proceedings of the ASME 2010 3rd Joint US-European Fluids Engineering Summer Meeting and 8th International Conference on Nanochannels, Microchannels, and Minichannels
FEDSM-ICNMM2010
August 1-5, 2010, Montreal, Canada

FEDSM-ICNMM2010-31025

STUDY THE INFLUENCE OF POSITION AND THE ANGLE OF THE WINGLETS ON MITE MICRO AIR VEHICLE

Babak Ganji
Aerospace Engineering Department, Amirkabir University of Technology;
Tehran, Tehran, Iran
ganji.babak@gmail.com

Romina Sadr-Eshkevari
Department of Information Technology, Maharashtra Institute of Technology;
Pune, India.
romina.sadr@yahoo.com

ABSTRACT

In recent years, small aircraft has been thoroughly studied and superior designs have been extensively developed. The aerodynamic design of micro aerial vehicles (MAVs), the most important small aircrafts, in Low-Reynolds number flow (LRNF) has become one of the main concerns to the profession. LRNF is mostly influenced by the airfoil design. Similar to all aircrafts, vertical elevons and winglets play an important role in the aerodynamics of MAVs. On this basis, the present study aimed to assess the effect of lateral angle alterations of the two vertical winglets in the aerodynamics of micro tactical expendable (MITE) in LRNF. A finite element flow solver (FEFS) based on structured grid was employed for studying the aerodynamic characteristics of MITE. The findings of the present study suggest that with the gradual increase in cant angle φ, lift force decreases and drag force remains unchanged. Also with the increase of lateral angle θ, drag force increases significantly and negligible changes are observed in lift force. Vertical elevons play an important role in the control of MITE. Also the effect of Reynolds number on aerodynamic coefficients is discussed.

Keywords: Aerodynamics; Cant Angle; Computational Fluid Dynamics; Drag Force; Finite Element Flow Solver; Lift Force; Low Reynolds Number Flow; Micro Aerial Vehicles; Micro Tactile Expandable; Winglet.

INTRODUCTION

The aerodynamics of air vehicles in low Reynolds number flow (LRNF) has been increasingly studied during the last two decades. LRNF has been applied in designing and development of micro air vehicles (MAVs). MAVs are remotely controlled unmanned air vehicles (UAVs) with low target dimensions used for remote observations and explorations. Potential expected improvements of MAVs include a maximum length of 15 cm, a target dimension of 10 km, a 30 minute continuous flight, and an 18 g capacity. Despite the early belief, designing MAVs is not confined to a mere reduction in the dimensions of unmanned vehicles. Since MAVs fly in LRFN, their aerodynamics is completely different from that of other aerial vehicles.

In independent studies, the aerodynamics of MAVs has been analyzed according to computational fluid dynamics (CFD). Ramamurti et al [1-4] analyzed the aerodynamic effect of the positioning of wings and propellers based on the computerized stimulation of micro tactical expendable (MITE) 2. In 1989, XFOIL code was introduced by Drela to analyze airfoil within viscous conditions. [5]

The present study aimed to assess the aerodynamics of flight within the LRNF and low viscosity regimens. Therefore it was decided to study the effect of lateral angulations of vertical winglet (installed on the main wing) on the aerodynamics of MITE [6], a promising type of MAV. Also the effect of Reynolds number on the lift and the drag coefficients was assessed. A structured grid was created and a corresponding finite element flow solver (FEFS) was

employed for studying the aerodynamic characteristics of MITE.

NOMENCLATURE

Φ Cant angle
θ Lateral angle
α Angle of attack
L Lift force
D Drag force
C_L Lift coefficient
C_D Drag coefficient

MODEL DESCRIPTION

The basic MAV model studied here was designed at Naval Research laboratory (NRL) and is named the Micro Tactical Expandable (MITE). MITE has a wingspan of 6 inch and a span/wing chord aspect ratio (AR) of 1.25. It is single-engine driven and has two counter-rotating propellers. The main airfoil is a National Advisory Committee for Aeronautics (NACA) 0006 section (NACA 0006 Airfoil). The end plates are NACA 0015 sections (NACA 0015 Endplates). The configuration control surface is a wedge airfoil. The wedge airfoil functions both as an aileron and a rudder [1, 6]. Figure 1 scheme the described configuration.

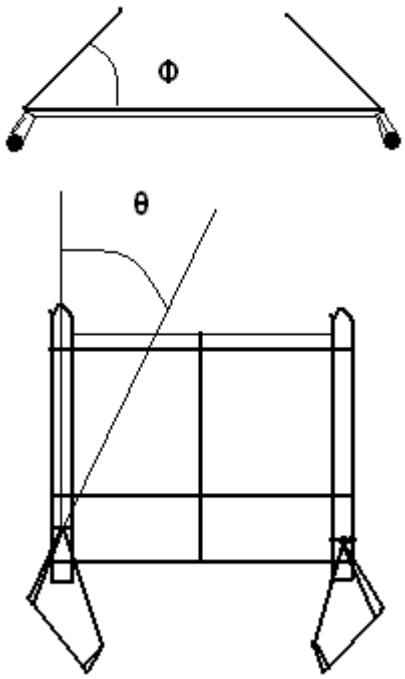

FIGURE 1. SCHEMATIC ILLUSTRATION OF MITE SHOWING THE CONTROL SURFACE ANGLES.

MESH GENERATION

FEFS was used. A structured grid was applied to improve the accuracy of the calculated C_D. C-type method was followed to generate the mesh. Measurements were performed on half of the MITE simulated symmetrical model. Mesh size was not even throughout the model: due to the high velocity and pressure gradients and the unsteady flow, a smaller mesh size was used for the simulation of trailing edge and wing angles. For other areas, however, mesh size was selected to be larger. Due to the unsteadiness of the flow at separation point, MITE simulation turned out to be challenging. Generally, it is almost impossible to predict the behavior of unsteady flow due to its inherent turbulence. Turbulent flow models are only valid for very simple geometries. For more complicated geometries, estimation is the only possibility.

BOUNDARY CONDITIONS

LRNF and the low velocity applied in the present study indicated that incompressible flows are being dealt with. Inlet velocity boundary condition was then used to determine the inlet velocity and the characteristics of the flow scalar. Four boundary conditions were defined:

1. Wall Boundary Condition (WBC)

WBC was used to limit the fluid or solid areas. For viscous flows, the non-sliding wall condition should be observed. Shear stress boundary condition was applied. For steady flow, the shear stress boundary condition by vertical velocity gradient is defined as:

$$\tau_w = \mu \frac{\partial v}{\partial n} \quad (1)$$

It should be noted that with a high velocity gradient in the wall, the grid should have sufficient accuracy and quality in order to correctly solve the boundary layer equations. The WBC was then used for the wings.

2. Symmetry Boundary Condition (SBC)

For SBC, the derivation of all variables is assumed =0 while passing symmetrical boundaries. Thus there would be no thermal flow flux (TFF) in a given symmetrical plane, meaning the normal component of the velocity would be zero in this plane. Also there would be no diffusion flux (DF) around the symmetrical plane. In other words, all normal gradients of flow variables will be =0. In summary:

- The vertical velocity component is zero:

$$v_n = 0 \quad (2)$$

- All normal gradients of the flow variables are zero:

$$\frac{\partial}{\partial_n} = 0 \tag{3}$$

3. Velocity Inlet Boundary Condition (VIBC)

VIBC is used along with all dependent scalar flow variables to define flow velocity in flow inlets. FEFS uses velocity components and scalar values to calculate inlet mass flow rate and momentum when the inlet velocity boundary condition has been defined to enter the physical field: The mass flow rate applied to a cell in close proximity of the inlet velocity boundary is defined as:

$$\dot{m} = \int \rho \vec{v}.d\vec{A} \tag{4}$$

Only the velocity component perpendicular to the control volume surface influences the mass flow rate.

4. Pressure Outlet Boundary Condition (POBC)

POBC uses the characteristics of the static pressure in the outlets boundaries. The determined static pressure values are only used in subsonic flows. The total pressure for incompressible flows is defined as:

$$P_0 = P_s + \frac{1}{2}\rho|\vec{v}|^2 \tag{5}$$

The static pressure value for supersonic flows or when the basic quantification is based on static pressure should be emphasized on.

SOLUTION RESULTS

Grid Study

Figures 2 and 3 illustrate the grid convergence in two states of steady and turbulent flows.

The results of C_L and C_D with a zero angle of attack were analyzed in four conditions:

1. Viscous flow with $Re = 10^5 (V = 13.24\,{}^{m}/_{s})$
2. Steady flow with $Re = 5 \times 10^4 (V = 6.62\,{}^{m}/_{s})$
3. Steady flow with $Re = 10^5 (V = 13.24\,{}^{m}/_{s})$
4. Turbulent flow with $Re = 10^5 (V = 13.24\,{}^{m}/_{s})$

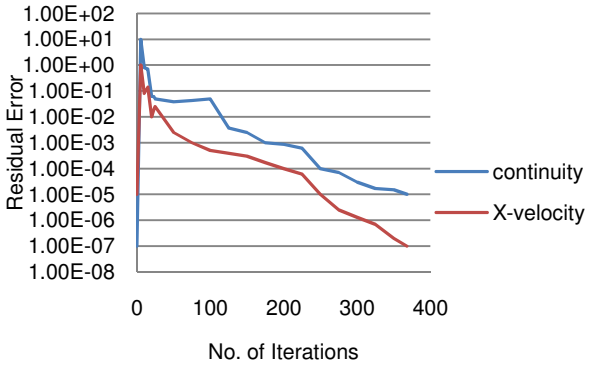

FIGURE 2. GRID CONVERGENCE HISTORY ASSOCIATED WITH STEADY FLOW, REYNOLDS NUMBER 10^5 AND ANGLE OF ATTACK =0.

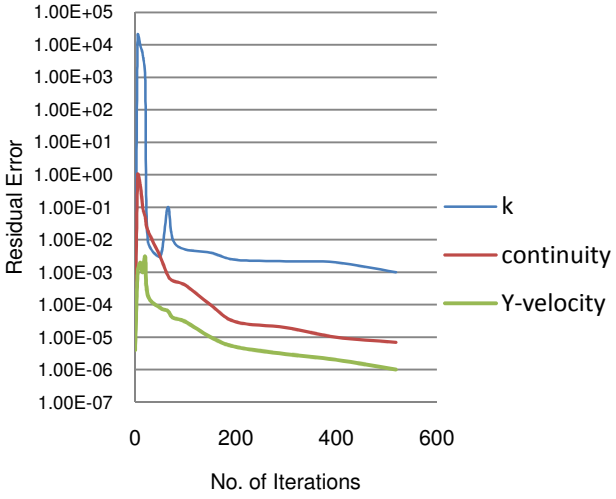

FIGURE 3. GRID CONVERGENCE HISTORY OF TURBULENT FLOW, $Re = 10^5$ AND A 0 ANGLE OF ATTACK.

Table 1 implies a decreased ${}^{L}/_{D}$ in steady state with $Re = 50000$ compared to that of viscous flow. This is thought to be attributed to the viscous drag effect. ${}^{L}/_{D}$ Of steady flow increases with Re due to the increased lift force and the negligible decrease of drag force. For Turbulent states, the model was assumed to be in a fully turbulent flow. The drag force increases slightly compared to that of steady flow due to the pressure and viscous elements. The lift force slightly decreases with ${}^{L}/_{D}$.

TABLE 1. THE C_L AND C_D ALTERATIONS AT ZERO ANGLE OF ATTACK.

Re	Lift Force	Drag Force	L/D
Viscous	6.62e-2	9.56e-3	6.92
Re=50000, Laminar	4.72e-3	2.38e-2	1.98e-1
Re=100000, Laminar	1.05e-2	1.92e-2	5.5e-1
Re=100000,Turbulent	2.86e-3	5.86e-2	4.88e-2

The effect of lateral angle alterations

The effect of cant angle (φ) alteration. Cant angle is shown in figure 1. To assess the angular effect of φ, MITE grid was created in different φ angles (0, 20, 40, and 45 degrees). Figure 4 shows the aerodynamic characteristics evaluated in different φ angles (0, 20, 40, and 45 degrees) and at various angles of attack, ranging from 0 to 15 degrees. These illustrations show an expected linear increase in lift force with increasing leading angle. Measurements show that $^{L}/_{D}$ proportion is maximum around $\alpha = 5$ and $0 < \varphi < 20$. The results show that $^{L}/_{D}$ proportion increases when φ decreases from 45 to 20. This is due to the increased lifting force in $\varphi = 20$ angle. The drag force value is constant for all φ angles. According to C_D, it may be concluded that the behavior of this diagram is similar to that of a quadratic equation. In other words, the growth of C_D increases with increased angle of attack. This is thought to be attributed to the increased pressure drag when angle of attack is present.

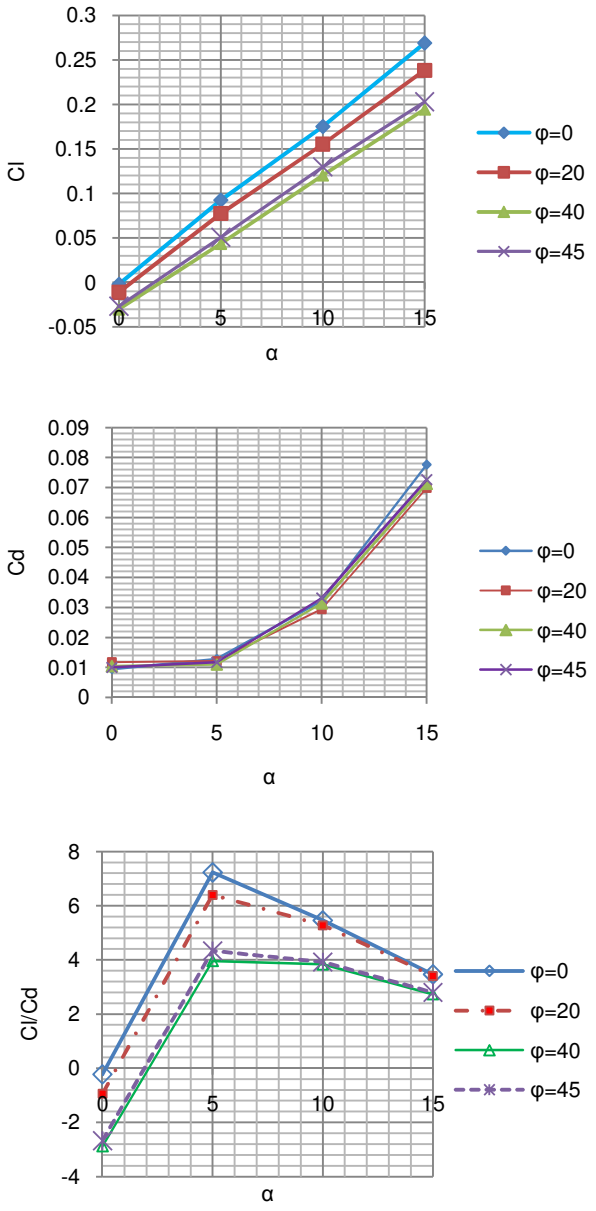

FIGURE 4. EFFECT OF Φ ANGLE ALTERATION ON LIFT AND DRAG.

The effect of θ angle. Θ is shown in figure 1. To assess the angular effect of θ, MITE grid was created in different θ angles (0, 20, and 45 degrees). Figure 5 shows C_L and C_D.

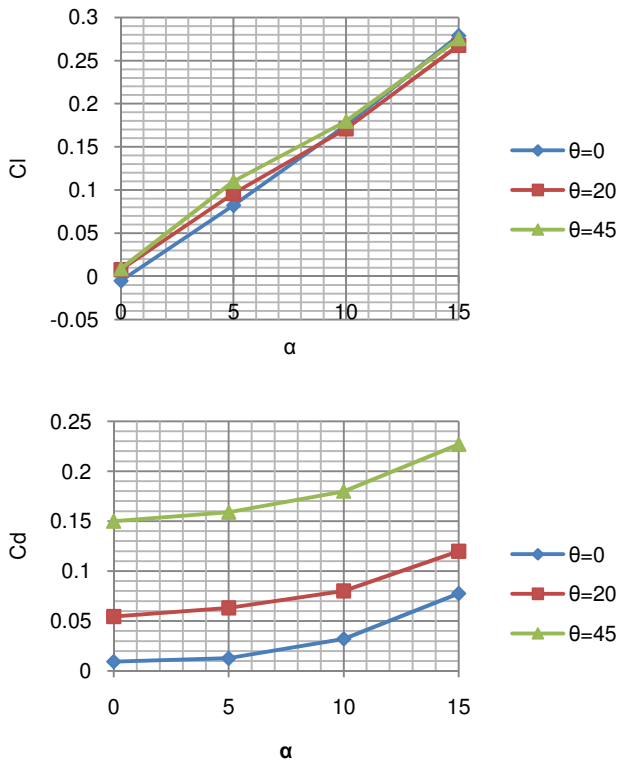

FIGURE 5. EFFECT OF Θ ANGLE ALTERATION ON LIFT AND DRAG.

Diagrams indicate that θ angle alteration has no significant influence on the lifting force. This seems to be correct according to the position of winglet during angle alteration. The surface facing the flow slightly changes to create lift force with altered angle. The C_D, however, shows a significant change in drag force with θ alterations. It is shown that when θ is changed from 0 to 20, C_D diagram places higher on the vertical axis. C_DValue also increases when θ is changed from 20 to 45. The only difference is that in the latter, the magnitude of increase is higher than that of the former. It may be concluded that with increased θ, the surface area facing the flow is increased. The greater the angle, the more significant the effect of the surface. To validate this assumption and further assess the angle, the vertical winglet was sectioned and the velocity contour and the vector of θ=0 and θ=20 with a leading angle of zero were traced. The resultant contour and velocity vector are shown in figure 6.

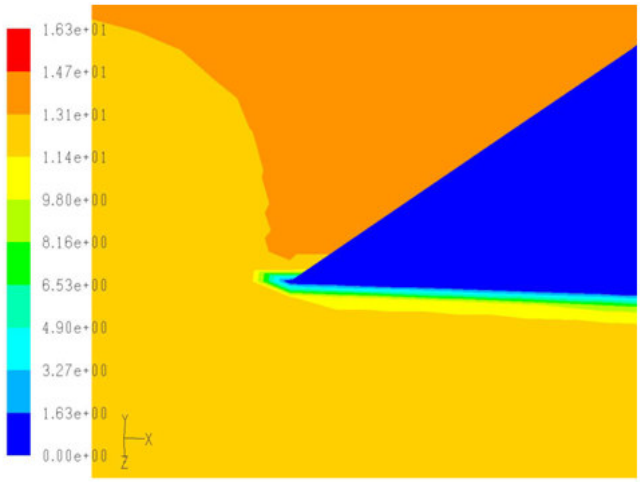

FIGURE 6-1A. CONTOURS OF VELOCITY AT WINGLET EDGE FOR LAMINAR FLOW, RE=100000, A=0, Θ=0.

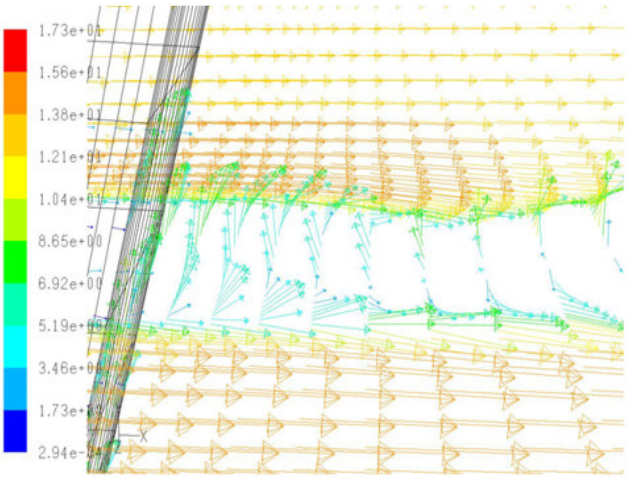

FIGURE 6-1B. VELOCITY VECTORS AT WINGLET EDGE FOR LAMINAR FLOW, RE=100000, A=0, Θ=0.

The contour of velocity and pressure indicate that in the vertical winglet to fuselage attachment the flow becomes turbulent when infinite flow is present. This results in the formation of different levels of pressure and velocity. In front of and behind the winglet, however, there seems to be an infinite flow recycling and a proper lamination of contour. Also the velocity vectors show a relatively turbulent flow behind the winglet. However, the reverse flow will never become completed because the vectors behind and near the winglet are perpendicular to the surface but will not be reversed. Further, velocity vectors will share the same direction and the infinite flow.

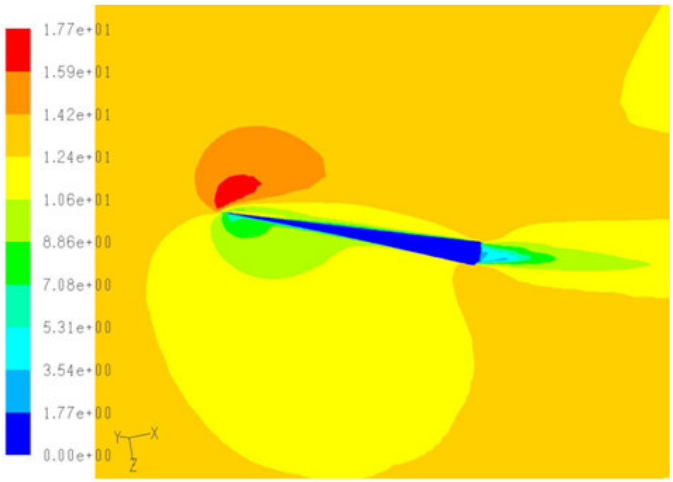

FIGURE 6-2A. CONTOURS OF VELOCITY AT WINGLET FOR LAMINAR FLOW, RE=100000, A=0, Θ=20.

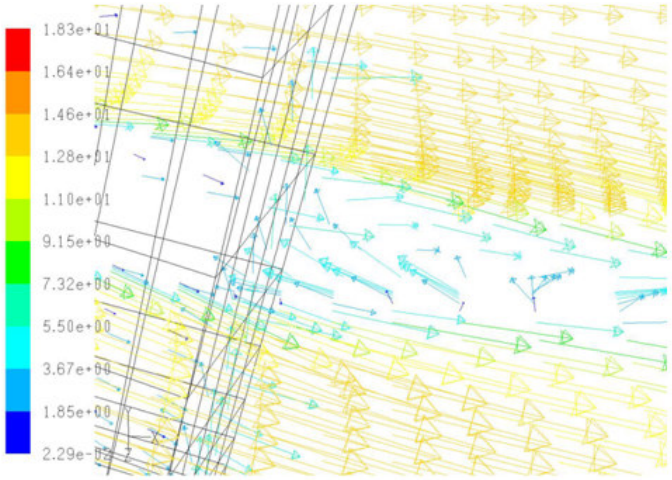

FIGURE 6-2B. VELOCITY VECTORS AT WINGLET FOR LAMINAR FLOW, RE=100000, A=0, Θ=20.

Due to the increased number of velocity and pressure contour surfaces in the anterior (in front) and posterior (behind) the winglet to fuselage connection, the turbulence is more significant at θ=20 (figure 6-2). Behind the winglet, the reversed flow is evident. The velocity vectors, compared to the flow vectors, show different and even opposite directions. In conclusion, it seems that flow separation and turbulence formation is much greater in 20 degree angle compared to that of zero degree. The turbulences result in increased pressure drag, and consequently increased total drag.

Comparison of the measured C_L and C_D of the grids with vertical winglet and those without. C_L and C_D of grids with vertical winglets were compared to those of the grids without vertical winglets (NACA 0006 airfoil [5, 7]). The results for different angles of attack are shown in figure 7.

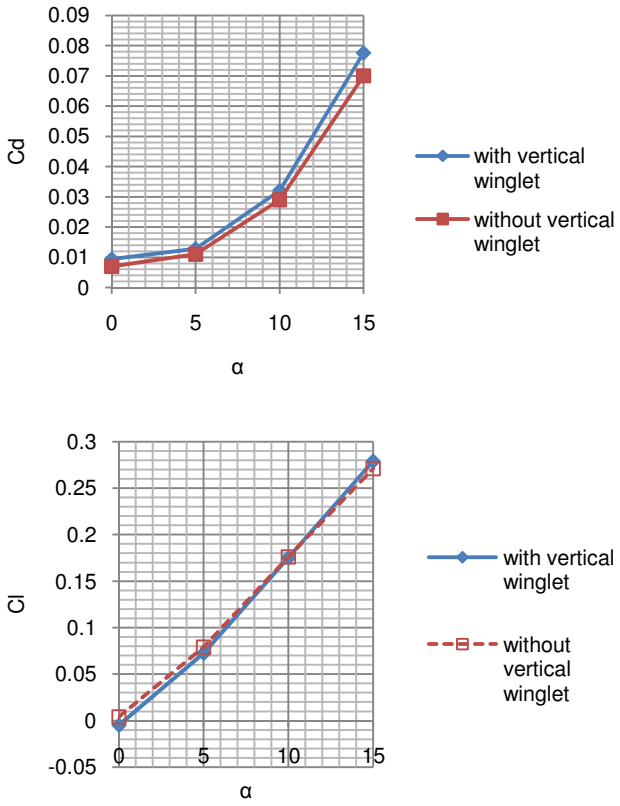

FIGURE 8. C_L AND C_D IN GRIDS WITH AND WITHOUT VERTICAL WINGLET.

The C_L diagram does not yield notable results. However, the effect of vertical winglet on drag force is evident from the C_D diagram. This effect is revealed with increased drag force in all angles of attack. This increase is attributed to the positioning of winglet. When winglets are placed into horizontal flows, total drag is increased.

DISCUSSION

It should be noted that MITE does not stall at high angles of attack (α=15). This is evident on the C_L diagrams. MITE has shown to successfully maintain high angles of attack in velocities under 4 $^m/_s$. [2] This is thought to be attributed to the delayed flow separation: the flow generated by propellers on the superior surface of the wing along with the ability of one wing with low AR in high angles of attack results in delayed flow separation. Since the effect of propellers was not concerned, low AR is the only reason behind the flow separation in the present study.

According to the fact that the mass center of MITE is located in %20 (one fifth) chord point (ahead of the forward limit), the moment arm of the vertical winglets (elevator) is further extended. For the same reason, vertical winglets can be used as proper controlling measures.

Winglet positioning during angle alteration influences the aerodynamics of flight. When angle is changed the surface

area facing the flow undergoes slight alteration. The opposite happens for the C_D: Drag force significantly increases with θ. This is due to the fact that the surface area facing the horizontal flow alters significantly. In other words, the surface area facing the flow increases with θ. When angle is increased from 0 to 20 degrees, the vortex behind the winglet increases significantly and a consequent flow separation happens. These vortexes results in an increased pressure drag and consequently an increased total drag. This phenomenon is even more significant when angle is changed from 20 to 45.

CONCLUSION

Within the limitations of the present assessment:

- L/D Reduces in steady state flow compared to that of viscous flow due to the viscous drag.
- L/D Increases with Re due to increased lift force and decreased drag force.
- L/D Decreases in turbulent flow due to the increased drag force as a result of pressure and viscous elements.
- L/D Value reaches its maximum when $0 < \varphi < 20$ with a leading angle of 5 degrees.
- C_L Decreases with φ while C_D slightly change.
- Slight change in C_L happen with θ changes from 0 to 20. These changes are of greater magnitude when angle is changed from 20 to 45.

REFERENCES

[1] Ramamurti, R., Sandberg W.C., and Löhner, R., 2000, "Simulation of the Dynamics of Micro Air Vehicles," *AIAA paper,* AIAA-2000-0896.

[2] Mueller, T.J., Kellogg, J.C., and Shkarayev, S.V., 2006, "Introduction to the Design of Fixed-Wing Micro Air Vehicles Including Three Case Studies," *AIAA Education Series.*

[3] Ramamurti, R., and Löhner, R., 1992, "Evaluation of an Incompressible Flow Solver Based on Simple Elements," *Advances in Finite Element Analysis in Fluid Dynamics, FED Col.137,* Dhaubhadel, M.N., et al., ed., American Society of Mechanical Engineers, New York, pp. 33-42.

[4] Ramamurti, R., Löhner, R., and Sandberg, W.C., 1994, "Evaluation of Scalable 3-D Incompressible Finite Element Solver," *AIAA Paper,* AIAA-1994-0756.

[5] Drela, M., 1989, "XFOIL: An Analysis and Design System for Low Reynolds Number Airfoils, *"Low Reynolds Number Aerodynamics, Lecture Notes in Engineering Vol. 54,* Mueller, T. J., ed., Springer-Verlag, New York, pp. 1-12.

[6] Kellogg, J., Bovais, C., Dahlburg, J., Foch, R., Gardner, J., Gordon, D., Hartley, R., Kamgar-Parsi, B., McFarlane, H., Pipitone, F., Ramamurti, R., Sciambi, A., Spears, W., Srull, D., and Sullivan, C., 2002, "The NRL Mite Air Vehicle, *"The Aeronautical Journal, Vol. 106(1062),*pp.431-441.

[7] Drela, M., and Giles, M.B., ISES: A Two-Dimensional Viscous Aerodynamic Design and Analysis Code, *AIAA Paper 87-90424*, Jan. 1987.

[8] Mueller, T.J., 1999, "Aerodynamic Measurements at Low Reynolds Numbers for Fixed Wing Micro-Air Vehicles, *"TO AVT/VKI Special Course on Development and Operation of UAVs for Military and Civil Applications.*

[9] Kevin, A., 1997, "Micro Air Vehicle (MAV) Development at NRL," *Association of Unmanned Vehicle Systems International Conference (AUVSI'97),* Arlington, VA, USA.

[10] Abdulrahim, M., and Cocquyt, J.B., 2002, "Development of Mission capable Flexible-Wing Micro Air Vehicles,"*53rd Southeastern Regional Student Conference,* Huntsville, Al., USA.

[11] Zimmerman, C. H., 1947, "Airplane of Low Aspect Ratio," *U.S. Patent Number2431293 (11-18-47)*